PROCEEDINGS A

royalsocietypublishing.org/journal/rspa

Research

Check for updates

Article submitted to journal

**Subject Areas:**
Biomedical engineering, Computer models and simulations, Biomechanics

**Keywords:**
epi-off crosslinking, cornea stiffening, in-depth stromal stiffening, analytical formulae, finite element simulations

**Author for correspondence:**
Anna Pandolfi, Alessandra Bonfanti
e-mail: anna.pandolfi@polimi.it, alessandra.bonfanti@polimi.it

# A predictive model of UV-A-riboflavin crosslinking treatment on porcine corneas

Alessandra Bonfanti[1] and Anna Pandolfi[1]

[1]Department of Civil and Environmental Engineering, Politecnico di Milano, Piazza Leonardo Da Vinci, 20133 Milan, Italy

The crosslinking technique (CXL) is an effective low-risk therapeutic treatment of keratoconus and other ectatic disorders of the human cornea. The effect of corneal CXL is to increase the stiffness of the stroma to prevent the progression of the cornea distortion. Several clinical and experimental studies have shown that the stiffening effects predominantly localise on the anterior portion of the stroma and that the in-depth stiffening distribution is highly dependent on the duration of treatment. Yet, how the stiffening effects distribute through the cornea thickness as a function of the treatment duration is an open question. Here we propose an analytical model of the stiffening profile due to CXL-treatment as a function of the irradiation time. We consider linear and nonlinear variations of the crosslinking effects across the thickness and implement them into a finite element model of the porcine cornea. We present a time-dependent in-depth stiffening profile that allows us to predict the post-operative corneas response to physiological intraocular pressure for different irradiation times. We anticipate that this predictive model will support the development of patient specific 3D models that will allow clinicians to design customised CXL treatment, thus enhancing treatment outcomes.



THE ROYAL SOCIETY PUBLISHING

## 1. Introduction

The crosslinking technique (CXL) is an effective low-risk therapeutic treatment of keratoconus and other ectatic disorders of the human cornea. Keratoconus is characterised by thinning and distortion of the cornea in a cone-like shape. CXL consists in the photo-polymerization of the collagen fibrils of the stroma. The stroma, de-epithelialized (epi-off) and soaked with riboflavin, which acts as photosensitizer, is exposed to ultra-violet-A (UV-A) radiation for a prescribed lapse of time [1]. The effect of corneal CXL is to increase the stiffness of the stroma to prevent the progression of the cornea distortion [2]. The precise molecular process involved in corneal CLX that lead to its stiffening is not fully understood, although it is clear that the central role is played by the formation of covalent bonds between fibrils due to UV-A-induced radical ions and singlet oxygen [3,4]. In-vitro studies have shown that the combination of riboflavin and UV-A irradiation causes two types of crosslink, i.e., between various collagen molecules (both intra-fibrillar and inter-fibrillar) and between proteoglycan core proteins [5]. While CXL treatment is already a clinically effective procedure, current effort focuses on (i) further improving CXL outcome, and (ii) on optimising the medical protocol to reduce the duration of treatment—thus lower the costs—and to reduce patients discomfort—pain.

Different modifications may be introduced in the cornea CXL protocol, yet not all available strategies result into an enhancement of the cornea stiffness. Clinical studies showed that use of pulsate UV-irradiation produces the same—or only slightly better—depth of penetration of cornea stiffening with respect to continuous irradiation [6]. Further, it has been clinically demonstrated that combination of a high-irradiance for short-time treatment significantly reduces the stiffening effect on the cornea, probably due to lack of tissue oxygen and increment of tissue damage [7,8]. A theoretical model able to compute the concentration of newly created collagen cross-links, directly responsible for the corneal stiffening, has been introduced [9]. The model relates the increment factor of stiffness due to CXL treatment as a function of irradiation time and stromal depth, riboflavin and oxygen diffusion, and riboflavin concentration. Interestingly, the theoretical model supported by experimental data, revealed that the effect of CXL depends more on the duration of the irradiation than on the overall applied UV-A intensity (fluence). A recent experimental study on pressurised porcine corneas tested the stiffening effect of different irradiation time (2.5, 5, 10, 15, 20 minutes) of de-epithelialised corneas [10]. Results demonstrated that the duration of the irradiation has a marked effect on stromal stiffening, in agreement with the previous theoretical model.

Several studies have shown that the stiffening effects due to CXL predominantly localise in the anterior portion of the stroma and no effect are observed on the posterior side of the cornea, see, e. g., [11]. Thus, the stiffness distribution within the cornea cross-section post CXL treatment is highly inhomogeneous. Recently, the depth and the distribution the stiffening effect across the corneal thickness induced by standard collagen CXL in porcine corneas was assessed by atomic force microscopy (AMF) [12]. Corneas were treated following the Dresden CXL protocol (30 minutes of irradiation with 3 mW/cm2 irradiance [1]) and they were not removed form the eyeball, thus they were pressurised at 36 mmHg intraocular pressure (IOP). At the end of the CXL treatment, AFM tests were performed at different thickness depths of excised cryofrozen corneal strips. Experimental measurements showed that the mean depth of the CXL stiffened zone for 30 minutes treatment was $1/3$ of the cornea thickness. Further, experimental data indicated that the variation of the stiffness, as a function of the depth from the anterior surface, were well-fitted by an exponential function.

It is well established that the stiffening effect due to CXL treatment is highly dependent on the duration of treatment and that the stiffness distribution within the cross-section is inhomogeneous. A recent numerical study attempted to provide a relationship between the stiffness depth of penetration and the treatment duration [13], by making use of the experimental

data presented in [10]. To limit the introduction of arbitrary fitting coefficients, the through-thickness CXL stiffening of the cornea was assumed as piece-wise-constant. The piece-wise-constant profile was converted in the stiffness coefficients of the material model for the cornea and used in a finite element simulations to predict the cornea apex displacement when subjected to physiological intraocular pressure (IOP). The finite element model accounting for a piece-wise-constant material properties distribution could fit the apex displacement of the inflated cornea. Yet, the material properties pre and post CXL treatment had to be independently calibrated. Unsurprisingly, the approximation was not satisfying, since (i) pre-CXL stiffness was assumed to be uniform, and (ii) the CLX stiffening profile was way too far from the actual distribution of post CXL stiffness. Similarly, a photo-chemical-mechanical model of one-dimensional crosslinking process across the corneal thickness, implemented into a coupled multi-physics finite element code, was applied to the solution of the three-dimensional boundary value problem of the CXL treatment. The study simulated the pressurization tests on untreated and post-CXL corneas of porcine eyes. The model successfully reproduced the experimental data reported in [14]. Yet, the material properties pre and post CXL treatment had to be independently calibrated.

With the ultimate goal of building a patient specific 3D model that will allow clinicians to design customised irradiation times for CXL treatment, in this study we investigate the stiffening profile due to CXL treatment within the cornea section as a function of the irradiation time. The aim of the present study is to develop a predictive model of the stiffness distribution within the cross section as a function of the treatment time by making use of experimental data available in the literature [10]. The combination of the predictive model developed here with a 3D finite element model reproducing patients cornea geometry will allow clinicians to customise clinical protocols, thus enhancing the outcome of the procedure while reducing recovery time and treatment costs.

The organization of the paper is as follows. In Section 2 we illustrate one model of stroma stiffness profile for untreated corneas and three models of profiles of the stromal stiffness for post-CXL corneas, and briefly recall the features of the finite element model used for the numerical simulation of the pressurization tests and the experimental data used in the study to validate the model (from [10]). In Section 3 we report the results of the calibration of the parameters of the one-dimensional models of stiffening, and the predictions of the numerical simulations of the pressurization tests in terms of corneal shape and stress distributions. In Section 4 we discuss the predictive properties of the models, commenting on its advantages and drawbacks, and draw some possible further advances or practical applications.

## 2. Materials and Methods

### (a) Experimental data

Here we summarize the experimental data that will be used for the validation of the predictive stiffness distribution model [10]. The results of pressurization experiments on crosslinked porcine corneas are reported in [10]. The study aimed at understanding the relevance on corneal stiffening of the duration of the irradiation (at 9 mW/cm2 fluence). Ninety corneas, inclusive of the limbus and of a small portion of the scleral ring, were de-epithelialized and pressurized from 0 to 30 mmHg before and after the CXL treatment. The corneas were subdivided in five groups; each group received the same amount of riboflavin, and a different irradiation time, i. e., 2.5, 5, 10, 15 and 20 minutes. The increment of stiffness was evaluated in terms of equivalent elastic modulus $E$, by interpreting the pressurization results through a classic linear model of spherical shells [15]. For each treatment group, the shell model was able to quantify the global effect of CXL with a unique number, i. e., the untreated cornea elastic modulus $E_b$, and post-CXL elastic modulus $E_a$. To extract these values, the cornea was considered as a spherical shell, with constant thickness, homogeneous, isotropic, and the presence of the stiffening limbus was neglected.

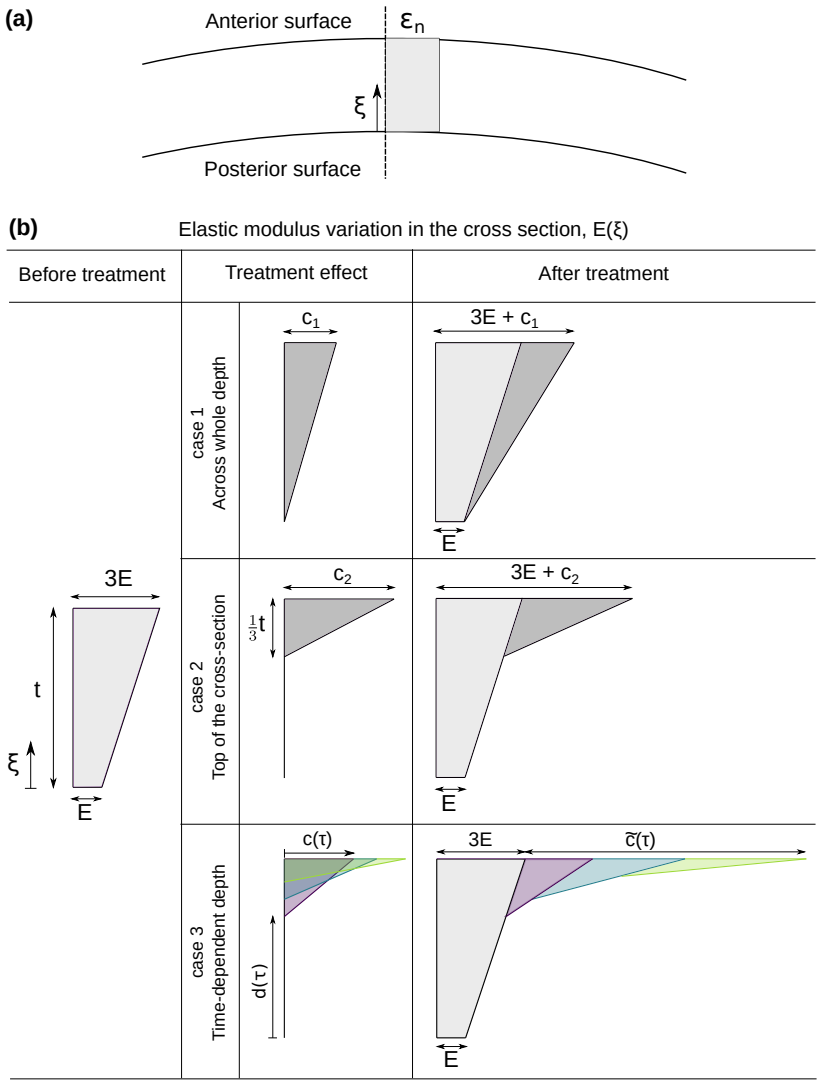


**Figure 1.** (a) Cross section of the cornea, of thickness $t$, assumed to experience a uniform strain distribution due to the membrane normal force. (b) Models of stiffness profiles. Before the CXL treatment, the elastic modulus follows a linear variation across the thickness, with the anterior value assumed to be three times the posterior value. The potential stiffening effect due to CXL treatment are analysed following three hypothesis: (1) the stiffening occurs within the entire cross section; (2) the stiffening is limited to the anterior 1/3 of the thickness; (3) the treatment penetrates up to a time dependent depth, i. e., the longer the cornea is UV-A-irradiated the less the stiffening effect can penetrate. The colours show the additional stiffening effect while time progresses. The elastic modulus through-thickness distribution after the CXL-treatment is given by the superposition of the two distributions, before and after the treatment.

## (b) Stiffness distribution model across corneal thickness

We consider one-dimensional models for the distribution of the normal stiffness across the corneal thickness $t$. In this derivation, we disregard the actual geometry of the cornea, which is characterized by a non-uniform thickness and non-isotropic curvature, and focus on the axial segment orthogonal to the anterior and posterior corneal apexes. Albeit curvature changes will occur because of the non uniform stiffness, we do not consider them and disregard the corresponding bending moment. We assume that the cornea balances the action of the IOP with a

normal stress $N_e$. Defining $\xi = z/t$, with $z$ a dimensional coordinate along the optic axis from the posterior surface and $0 \leq \xi \leq 1$ a dimensionless coordinate Fig. 1(a), we write

$$N_e = \int_0^t \sigma(\xi) d\xi \,.$$

According to the previous assumptions, the strain along the axial segment is uniform $\varepsilon(\xi) = \bar{\varepsilon}$, while the stress profile $\sigma(\xi)$ will be defined by the profile of the elastic modulus $E(\xi)$.

We consider an untreated stiffness profile varying linearly across the thickness. Based on previous clinical and experimental observations, we hypothesise three different stiffening profiles within the cornea cross-section: (1) the stiffening affects the entire thickness; (2) the stiffening affects only the anterior third of the thickness; (3) the depth at which the CXL stiffening occurs is dependent on the irradiation time: the longer the cornea is irradiated for, the less deep the stiffening effect is. The post-CXL elastic modulus profile along the axial segment is given by the superposition of untreated and post-CXL profiles.

### (i) Linear distribution of the stiffness before CXL-treatment

Let us assume that the pre-CXL elastic modulus varies linearly across the thickness, see Fig. 1(b). The profile assigns the unknown value $E$ at the posterior side and the value $cE$ at the anterior side, where $c$ is equal to 3. The coefficient $c = 3$ has been estimated from the results of experimental tests on corneal buttons [16]. We make use of the normal force equilibrium to determine the value $E$

$$N_e = \frac{1}{2}(3E + E)t\bar{\varepsilon} = 2\,E\,t\bar{\varepsilon} = E_b\,t\,\bar{\varepsilon}, \tag{2.1}$$

where $E_b$ is the average Young's modulus before CXL-treatment measured experimentally from tissue-level tests performed in [10]. From equation (2.1) we have

$$E = \frac{E_b}{2}\,. \tag{2.2}$$

The profile of $E(\xi)$ for untreated corneas is assumed to be

$$E^{\text{before}}(\xi) = \frac{E_b}{2}\,(1 + 2\,\xi)\,. \tag{2.3}$$

### (ii) Linear distribution after CXL-treatment

Clinical observations show that the CXL treatment has almost no effect on the posterior portion of the cornea, and the stiffening is dominant on the anterior portion. As a first model of stiffening profile, we assume a linear variation across the thickness, see Fig. 1(b) case 1. We consider the average increment of corneal stiffness $\Delta E = E_a - E_b$, where $E_b$ and $E_a$ are the average Young's modulus before and after CXL-treatment respectively measured experimentally from tissue-level tests [10]. The maximum value of the stiffness increment due to CXL is at the anterior surface, for $\xi = 1$, and it corresponds to $c_1 = 2\Delta E$. The increment profile across the thickness is

$$\Delta E_1(\xi) = 2\Delta E\xi\,. \tag{2.4}$$

Therefore, the final profile of the elastic modulus across the thickness after CXL-treatment is

$$E_1^{\text{after}}(\xi) = \frac{E_b}{2} + 2\left(E_a - \frac{E_b}{2}\right)\xi\,. \tag{2.5}$$

## (c) Linear distribution in the anterior third after CXL-treatment

Clinical data report that the long-term stromal stiffness induced by CLX localizes at the anterior third of the stroma. As a second model, we assume that effect of the CLX is confined to the anterior third of the thickness, reaching the maximum at the anterior surface, see Fig. 1 (b), case 2. In this

case, the maximum stiffness increase is given by $c_2 = 6\Delta E$, leading to the elastic modulus profile across the anterior one-third as

$$\Delta E_2(\xi) = 6\Delta E(3\xi - 2)\,, \qquad 2/3 \le \xi \le 1\,. \tag{2.6}$$

By superposition, the post-CXL bi-linear distribution of the Young's modulus within the cross section is

$$E_2^{\text{after}}(\xi) = \begin{cases} E_b(1+2\,\xi)/2\,, & 0 \le \xi < 2/3 \\ E_b(25/2 - 17\xi) - E_a(12 - 18\xi)\,, & 2/3 \le \xi \le 1\,. \end{cases} \tag{2.7}$$

| Irradiation | Experiments | | Before | After | | |
|---|---|---|---|---|---|---|
| | | | | Linear | 1/3 linear | Time-dep |
| (min) | $E_b$ | $E_a$ | $E$ | $c_1$ | $c_2$ | $\tilde{c}_3$ |
| 2.5 | 0.480 | 0.788 | 0.240 | 0.616 | 1.848 | 1.848 |
| 5.0 | 0.590 | 0.855 | 0.295 | 0.533 | 1.590 | 1.590 |
| 10 | 0.505 | 0.978 | 0.252 | 0.946 | 2.838 | 2.666 |
| 15 | 0.716 | 1.416 | 0.358 | 1.431 | 4.200 | 7.494 |
| 20 | 0.562 | 1.732 | 0.281 | 2.343 | 7.023 | 23.304 |

**Table 1.** Stiffness parameters in MPa. Average experimental data ($E_b$ and $E_a$), pre-CXL $E$, and post-CXL coefficients $c_1$, $c_2$ and $\tilde{c}_3$ for the three incremental stiffness profile models, and for each treatment group (rows).

### (i) Time-dependent penetration depth during CXL-treatment of the cornea

Ex-vivo experiments have revealed that the level of stiffening due to CXL increases as a function of the time of exposure to UV-A [12]. Also the experimental data from [10], visualized in Fig. 2(a) with a broken black curve, evidence a nonlinear increase of the stiffness with irradiation time.

These observations suggested a third model of the in-depth stiffening profile, where both the dimensionless depth of the treatment (measured from the posterior surface) $d(\tau)$ and the incremental stiffness $\Delta E(\tau)$ are assumed to be dependent on the UV-A irradiation time $\tau$, when the irradiation time exceeds a threshold time $\tau_0$. The model is visualized in Fig. 1(b), case 3. For irradiation times inferior to $\tau_0$, model 3 coincides with model 2.

In model 3, the CXL *reactive* depth, $1 - d(\tau)$, remains equal to $1/3$ of the corneal thickness up to $\tau_0 = 300$ s (5 minutes) of the UV-A irradiation. Afterwards, the reactive depth reached by the subsequent increases of stiffness decays exponentially, halving in 5 minutes, as shown in Fig. 2 (b), solid black curve. Only the foremost layers of the stroma, above $d(\tau)$, keep stiffening. According to this assumption, the depth $2/3 \le d(\tau) \le 1$, signaling the instantaneous demarcation between *reactive* tissue and the *non-reactive* tissue, depends on the irradiation time as

$$d(\tau) = \begin{cases} 1 - 1/3 & 0 \le \tau < \tau_0 \\ 1 - 1/3 \quad e^{-\mu(\tau - \tau_0)} & \tau \ge \tau_0 \end{cases}\,. \tag{2.8}$$

where $\mu = 0.0023\ \text{s}^{-1}$.

In order to attain an analytical expression for the model, the experimental curve of the incremental stiffness $\Delta E(\tau)$ is approximated with a second order polynomial of $\tau$, see the solid green line in Fig. 2(a). The polynomial reaches a minimum value $\Delta E_0 = 0.3$ MPa at $\tau_0 = 300$ s,

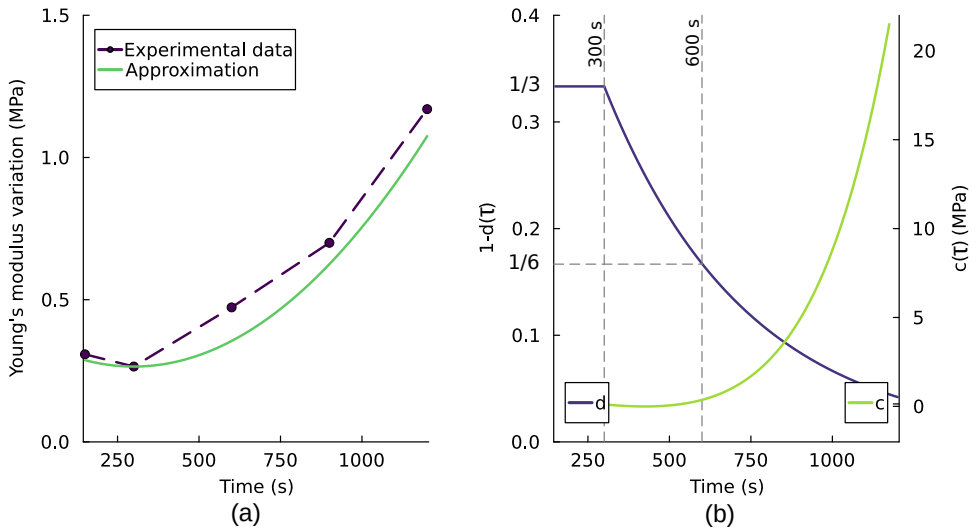


**Figure 2.** (a) Dependence of the difference $\Delta E$ between the post-CXL equivalent elastic modulus $E_a$ and the pre-CXL equivalent elastic modulus $E_b$ on the irradiation time. Experimental data (broken dashed black curve) versus analytical approximation (solid green curve). (b) Dependence of the constants $c_3(\tau)$ and $1-d(\tau)$ of the proposed model on the irradiation time.

and it holds only for $\tau \geq \tau_0$. The analytical expression of the incremental stiffness is

$$\Delta E(\tau) = E_a(\tau) - E_b(\tau) = \Delta E_{\text{inc}}(\tau - \tau_0)^2 + \Delta E_0\,, \qquad \tau \geq \tau_0\,, \tag{2.9}$$

where $\Delta E_{\text{inc}} = 10^{-6}$ MPa/s$^2$ is an equivalent stiffness acceleration.

Next, in order to derive a time dependent model, we consider to the instantaneous increase of the stiffness. By differentiating Eq. (2.9) with respect to $\tau$ we obtain the stiffness rate

$$\frac{\partial \Delta E(\tau)}{\partial \tau} = 2\Delta E_{\text{inc}}(\tau - \tau_0)\,, \qquad \tau \geq \tau_0\,. \tag{2.10}$$

In agreement with the previous models, now we assume that the stiffness rate is distributed linearly over the reactive depth, and write

$$\frac{\partial \Delta E(\tau)}{\partial \tau} = \frac{1}{2}\,(1 - d(\tau))\,c_3(\tau)\,, \qquad \tau \geq \tau_0\,, \tag{2.11}$$

where $c_3(\tau)$ (in MPa/s) represents the instantaneous increment of the stiffness at the anterior surface. By equating (2.10) and (2.11) and using (2.8), we obtain the explicit expression of the rate $c_3(\tau)$ as

$$c_3(\tau) = 12\,\Delta E_{\text{inc}}\,(\tau - \tau_0)\,e^{\mu(\tau-\tau_0)}\,. \tag{2.12}$$

It is easily verified that the incremental stiffness on the anterior portion of the stroma, $\Delta E(\tau)$, is obtained by integrating over the time Eq. (2.11) with $c_3(\tau)$ given by Eq. (2.12). Finally, the time-depending stiffening (in MPa) at the anterior surface of the stroma $\tilde{c}_3(\tau)$ is given by integrating $c_3(\tau)$ over the time as

$$\tilde{c}_3(\tau) = \int_{\tau_0}^{\tau} c_3(t)dt = \frac{12\,E_{\text{inc}}}{\mu^2}\left(1 + [\mu(\tau - \tau_0) - 1]\,e^{\mu(\tau-\tau_0)}\right)\,, \tag{2.13}$$

The anterior surface stiffness increases monotonically with the irradiation time as visualized by the green solid line in Fig. 2(b).

The stiffness profile $E_3(\xi, \tau)$ across the thickness cannot be obtained analytically, but it is computed numerically by adding at every depth the corresponding incremental stiffness due to

the progress of the irradiation. An animation of the progression of the stiffening profile is available in the Supplementary Material.

Table 1 collects all the parameters used by the three models, including the experiemental average elastic moduli $E_b$ and $E_a$, the posterior pre-CXL elastic modulus $E$, and the coefficients $c_1$, $c_2$ and $\tilde{c}_3$ of the three models of stiffening profiles.

### (d) Finite element model

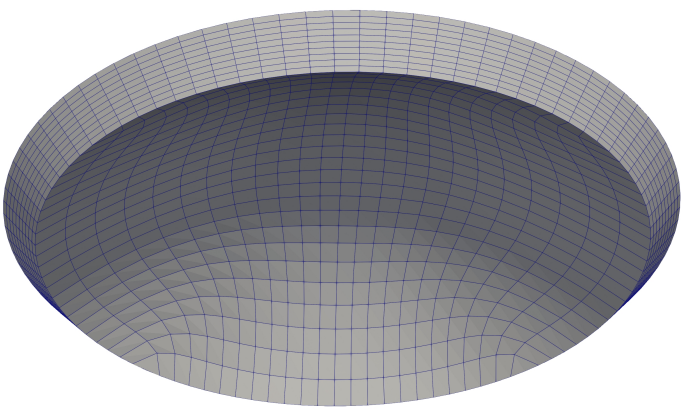

**Figure 3.** View of the finite element model of the cornea from the bottom side, showing the fine discretization across the thickness.

The one-dimensional profile of the stromal stiffness pre- and post-CXL described in the previous equations have been used to characterize the through-thickness stiffness of a finite element model of the human cornea [17]. The cornea model is robust and it has been applied to the simulation of refractive surgery [18], mechanical tests on the human cornea [19] and on pig corneas [13,20], by considering also the variation of the material stiffness across the thickness. The cornea model includes the typical features of the stromal tissue, i. e., finite kinematics, quasi-incompressibility, presence of distributed sets of collagen fibrils, to account for the natural variability observed in biological tissues. The material model is hyperelastic and anisotropic, locally characterized by seven parameters, briefly described in A.

For the present simulations, the geometric model has been constrained at the limbus and a growing pressure has been applied to the posterior surface of the cornea, to reproduce the boundary conditions of the laboratory experiments [10]. We created five different models, one for group of treatment, since the average geometry of each group was slightly different from the others. The geometry from each group was built on the basis of the average data of the corneas belonging to that group, measured in the unstressed configuration [13].

The geometry is discretized into 8-noded brick elements with linear interpolation, and comprises 10 layers across the thickness to allow the assignment of different material properties according to the depth. The total number of nodes is 6,875 and the total number of elements is 5,760. Fig. 3 shows one of the meshes adopted for the numerical analyses.

## 3. Results

We begin with the identification of the material stiffness of the untreated corneas with an in-depth linear profile of the cross-section stiffness according to Eq. (2.3). Using an average geometry extracted from experimental data [10], for each treatment duration group we performed a first set

of iterative analyses, and compared the average experimental apex displacement-IOP curve with the one obtained by the numerical calculations. For each group of corneas, the stiffness parameters (except for the bulk modulus $K$) were progressively updated, using the least square method to minimize the distance between numerical and experimental curves, but always following a linear profile uniquely identified by a single value $E$. Table 2 provides the values of the stiffness parameters, for each group, at the posterior side of the cornea, and the total error on the approximation (sum of the squares of the difference between experimental and numerical values). Details for the values assigned to each layer are reported in Table 3 in the Supplementary material.

The comparison between pre-CXL experimental and numerical results, in terms of IOP versus apex displacement curves, is reported in Fig. 4 for all five treatment duration, denoted with circles. The numerical response for untreated corneas shows the excellent agreement achieved with a linear stiffness profile for all cases.

| Irradiation (min) | $\mu_1$ (MPa) | $\mu_2$ (MPa) | $k_{11}, k_{12}$ (MPa) | $k_{21}, k_{22}$ | Error pre-CLX |
|---|---|---|---|---|---|
| 2.5 | 0.010 | -0.009 | 0.12 | 200 | 7.0e-4 |
| 5.0 | 0.010 | -0.009 | 0.20 | 200 | 3.6e-4 |
| 10 | 0.010 | -0.009 | 0.13 | 200 | 6.0e-4 |
| 15 | 0.010 | -0.009 | 0.22 | 200 | 2.2e-4 |
| 20 | 0.010 | -0.009 | 0.14 | 300 | 9.1e-4 |

**Table 2.** Material modelling parameters for each treatment duration for the posterior side of the cornea (parameters for all the 10 layers for the computational model are provided in Supplementary Materials). The bulk modulus is assumed 5.5 MPa [17]. The parameters are chosen so that the difference between experiments and simulations of the apex displacement before treatment is minimised.

Next, we compute the stiffening profile after CXL treatment for the three hypothesised models (linear, anterior third linear, and irradiation time-dependent) discussed in Section 2. The materials parameters across the cornea cross-section after CXL treatment were updated accordingly to the predicted stiffening profiles, by starting from those previously calibrated against the pre-CXL inflation curve on the posterior surface. For each treatment duration group we performed three numerical analysis, one for each predicted profile (linear, anterior third linear, and irradiation time-dependent). Tables 4-6 in the Supplementary Materials provide the individual values assigned to each layer for the three profile models, respectively.

The results of the numerical simulations and the experimental data for the post-CXL corneas, in terms of IOP-apex displacement curves (denoted with triangles), are shown in Fig. 4 for the profile models 1 and 2. The two models provide a satisfactory prediction for the cases below 5 minute irradiation. Fig. 5 shows the same results for the profile model 3 (which for irradiation times below 5 minutes is identical to the model 2, leading to the same results) revealing, for irradiation times above 10 minutes, a marked improvement with respect to the model 2, which is also shown in the plots.

For the corneas of the groups treated with 10 and 20 minute irradiation time–time-dependent model (model 3), Fig. 6 shows the distribution of the normal stress in the nasal-temporal direction across the thickness, at the physiological IOP, assumed to be 16 mmHg, comparing the pre-CXL case withe the post-CXL case. The presence of a stiffer layer causes an increment of the normal stress in the anterior portion of the cornea and a reduction of the stress in the posterior layers, which is more evident for the 20 minute case. A direct comparison of the nasal-temporal meridian

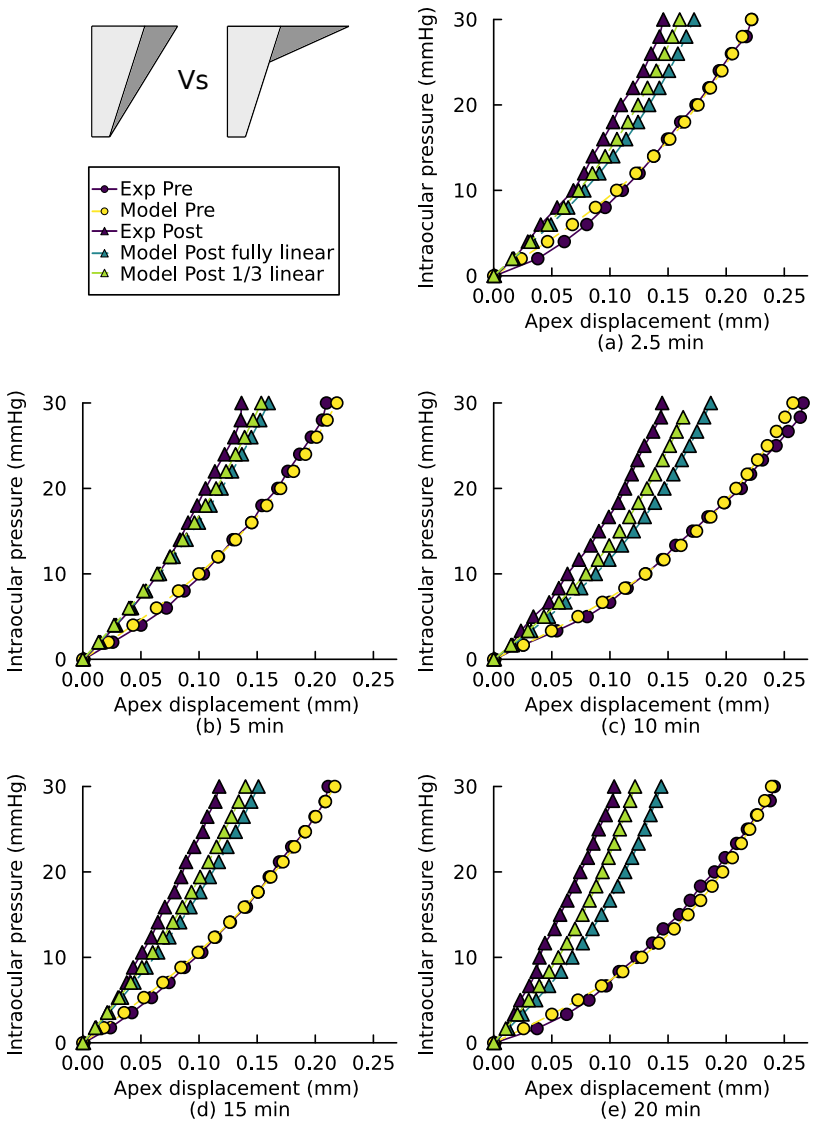


**Figure 4.** Prediction of cornea response to pressurization after the CXL treatment assuming that the treatment can penetrate within the whole cross section (case 1) or that the stiffening is limited to 1/3 of the cross section (case 2). The predictions are computer for different treatment times: (a) 2.5 minutes, (b) 5 minutes, (c) 10 minutes, (d) 15 minutes and (e) 20 minutes.

corneal profiles before and after the CXL, at the physiological IOP (16 mmHg) (Fig. 7) shows the less compliant behavior of the treated corneas. In the supplementary material it is possible to access to a short animation showing the predicted evolution with the irradiation time (according to the stiffness profile model 3) of the normal stress component in the nasal-temporal direction over a meridian corneal section.

## 4. Discussion and Conclusions

The stiffening of the corneal tissue due to CXL depends in a preponderant measure on the time of exposure to UV-A radiation. Furthermore, the stiffening affects the anterior layers of the cornea

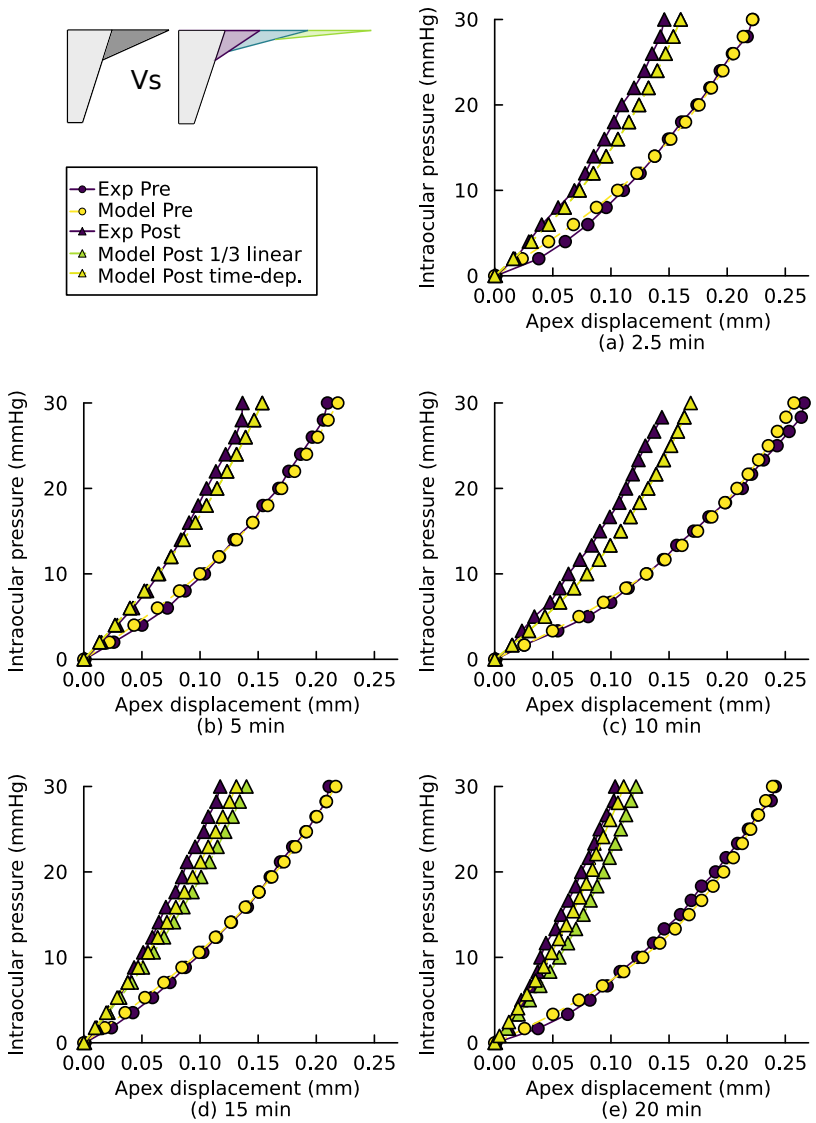


**Figure 5.** Prediction of cornea response to pressurization after the CXL treatment assuming that the stiffening is limited to 1/3 of the cross section (case 2) or that the stiffening penetration depth is time dependent (case 3). The predictions are computer for different treatment times: (a) 2.5 minutes, (b) 5 minutes, (c) 10 minutes, (d) 15 minutes and (e) 20 minutes.

and is less effective on the posterior layers. Clinical observation have pointed out the presence of a demarcation line, evident in the fist days after the CXL, that separates the portion of the cornea modified by the CXL treatment from the one practically untouched [11].

To assess the influence of the irradiation duration on the stiffening, an experimental campaign on ninety porcine corneas was presented in [10]. The study has some relevance, since the stiffening effect was quantified by means of tests that preserved the integrity of the tissue, unlikely other studies that were based on uniaxial tests on excised strips of previously CXL-treated corneas. The advantage of the chosen procedure was that pressurization tests pre-CLX and post-CLX could be performed on the same cornea, thus the actual reinforcement induced by the treatment could be quantified, since the uncertainties related to the biological variability were removed. The corneas were grouped in five groups, differing for the irradiation time, and the results of

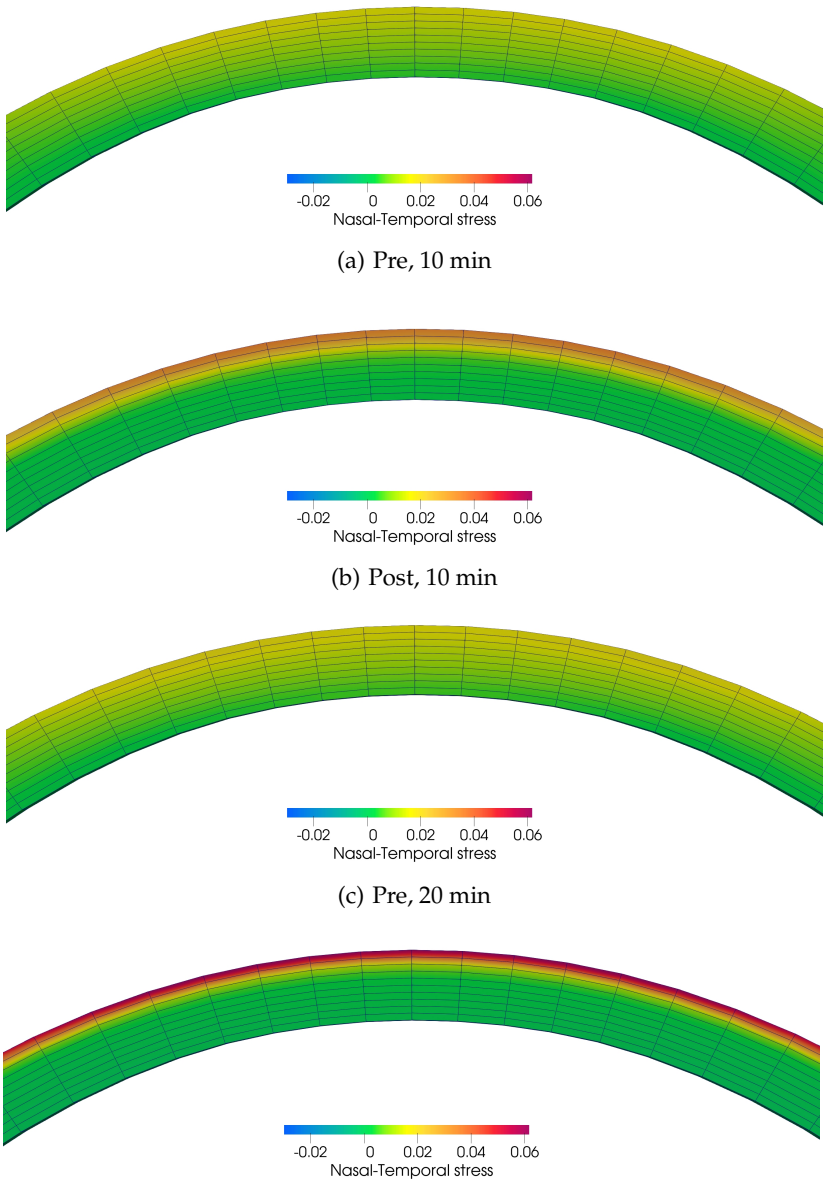


**Figure 6.** Numerical results, stiffness profile model 3, physiological IOP, 16 mmHg. Normal stress component in the nasal-temporal direction over the nasal-temporal meridian, before and after the CXL-treatment for the 10 and 20 minutes irradiation time.

the experiments were statistically characterized in both the pre-CXL and post-CXL conditions. Interestingly, the experiments on untreated corneas of each group revealed a different behavior in terms of average apex-displacement versus IOP plots, probably because the eyes were obtained by different groups of pigs. A simple interpretation of the results was provided by the linear shell theory in terms of an average (in the sense of average over the corneas of the group, and average over the non-homogeneity of the cornea) elastic modulus for the two conditions. On the basis of these two numbers, an attempt to describe the effect of CLX was presented in [13]. The assumption used in [13] was to have a uniform stiffening on the anterior layer of the cornea. Because of the

(a) 10 min

(b) 20 min

**Figure 7.** Numerical results, stiffening profile model 3, physiological IOP, 16 mmHg. Comparison of the pre-CXL corneal profile (green solid color) with the post-CXL profile (black lines) along the nasal-temporal meridian section, for the 10 and 20 minute irradiation cases.

simplifications involved, the model revealed to be not predictive. The way the anterior portion of the cornea is modified from the mechanical point of view was not well understood, except for the fact that with the progression of the irradiation time the stiffening did not occur in the deeper layers but only in the superficial ones [11].

In-vitro experiments conducted on excised strips of porcine corneas treated with CXL revealed that the stiffening of the tissue in the reinforced zone quickly decays from the anterior surface [12]. The information provided in [12] was of fundamental relevance and characterized statistically. Thirty measurements performed at every corneal depth, taken at 5 $\mu$m distance intervals, followed a log-normal distribution and were log-transformed to obtain the average. For practical reasons, AFM measurements were performed on unstressed tissue, obtained by excision of the pig corneas after CXL treatment. Qualitatively, the results underestimate the physiological stiffness of the tissue, since biological tissues reveal a growing stiffness with strain, but the qualitative trend revealed by the experiments was very clear. The results cannot be directly compared with the ones obtained in [10], because of the different testing conditions and loading state; we observe, in fact, one order of magnitude difference with respect to the present study.

The results in [12] suggest to revisit the original model of the piece-wise-constant CXL stiffening profile [13] to account for the variation with the depth. In all the models, we impose that the pre-CXL average stiffness equals the experimental elastic modulus $E_b$ and the post-CXL average stiffness equals the experimental modulus $E_a$. The stiffening profile is applied to all the stiffness coefficients of the finite element corneal model, except for the bulk modulus $K$, which has been set equal to 5.5 MPa for all the analyzed cases. The reason is that in our model $K$ is considered as a penalty coefficient to enforce incompressibility of the tissue, and its value should not be modified.

A linear variation of the stiffness increment (model 1), though, did not show a marked improvement with respect to the piece-wise-constant. A motivation of the scarce predictability is due to the fact that the model fails to describe the limited penetration depth of the CXL treatment. Limiting the increment of the stiffness to the anterior third (model 2) results into a more satisfactory prediction for short irradiation times ($\tau_0 \leq 5$ minutes), but for larger irradiation times

the post-CXL response deviates from the experimental one. The third model of stiffening profile was instead suggested by a critical observation of the numerical results with model 2, combined with clinical observations [11]. The depth of the CXL action depends on the time of exposure: the longer the cornea is subjected to UV-A irradiation, the thinner is the size of the effectively treated stroma. We introduced an incremental model of stiffening, whose effects on the cornea can be evaluated only by time integration. The model assumes that the action of irradiation on a time interval will be more and more limited to a superficial layer of the stroma. The assumption leads to a very interesting stiffening model, with high predictability which is able to cover the behavior of the five groups of corneas.

Interestingly, the time dependent profile model includes an exponential expression in time, which recalls the exponential function describing the profile of the elastic modulus as obtained by indentation tests in [12]. Note that our model transfers the exponential trend also to the depth, in agreement with [12].

The time-dependent stiffening profile (model 3), combined with an advanced finite element model of the cornea, provides a clear indication of the mechanical effects of CXL on the cornea. The anterior portion of the tissue is demanded to carry larger tensile stress, which are redistributed across the thickness, see Fig. 6, while the posterior portion is relieved and sustains smaller tensile stresses.

In the finite element model, a post-CLX reduction of the overall compliance of the cornea, which deform less under the same IOP, is observed, see Fig. 7. This behavior is explained by the hyperelasticity assumptions, for which the effect of modifying the stromal stiffness results into a retraction of the cornea with respect to the untreated configuration. A perfectly elastic behavior, that corresponds to the observation in the experiments on porcine corneas, may not be the one actually observed in clinics, since the CXL is performed on a degenerated tissue, and the stiffening effect does not involve the restoring of the healthy configuration of the cornea.

A natural question arising is how realistic and reliable is the extension of results obtained in experimental tests (whit the aid of numerical simulations) on porcine cornea to human corneas. Porcine corneas are rather similar to the human corneas in terms of mechanical behavior, but the geometrical and mechanical properties may be very different. The present results cannot directly be used to describe human eyes and an experimental campaign on human corneas is necessary to confirm the possibility to use this model in clinical applications.

Acknowledgements. The authors wish to acknoledge Politecnico di Milano for the Seal of Excellence Fellowship to support AB. The authors thank Dr. Cesare Fumagalli, President of Fumagalli Industria Alimentari S.p.A. for the supply of the pig eye used to collect the data set employed for the development of the present model.

## References

1. Wollensak G, Spoerl E, Seiler T. 2003 Riboflavin/ultraviolet-A–induced collagen crosslinking for the treatment of keratoconus. *American journal of ophthalmology* **135**, 620–627.
2. Spoerl E, Mrochen M, Sliney D, Trokel S, Seiler T. 2007 Safety of UVA-riboflavin cross-linking of the cornea. *Cornea* **26**, 385–389.
3. Wollensak G, Spoerl E, Seiler T. 2003 Stress-strain measurements of human and porcine corneas after riboflavin–ultraviolet-A-induced cross-linking. *Journal of Cataract & Refractive Surgery* **29**, 1780–1785.
4. Wollensak G, Wilsch M, Spoerl E, Seiler T. 2004 Collagen fiber diameter in the rabbit cornea after collagen crosslinking by riboflavin/UVA. *Cornea* **23**, 503–507.
5. Zhang Y, Conrad AH, Conrad GW. 2011 Effects of ultraviolet-A and riboflavin on the interaction of collagen and proteoglycans during corneal cross-linking. *Journal of Biological Chemistry* **286**, 13011–13022.
6. Mazzotta C, Traversi C, Caragiuli S, Rechichi M. 2014 Pulsed vs continuous light accelerated corneal collagen crosslinking: in vivo qualitative investigation by confocal microscopy and corneal OCT. *Eye* **28**, 1179–1183.
7. Hammer A, Richoz O, Mosquera SA, Tabibian D, Hoogewoud F, Hafezi F. 2014 Corneal biomechanical properties at different corneal cross-linking (CXL) irradiances. *Investigative*

*ophthalmology & visual science* **55**, 2881–2884.
8. Kanellopoulos AJ, Loukas YL, Asimellis G. 2016 Cross-linking biomechanical effect in human corneas by same energy, different UV-A fluence: an enzymatic digestion comparative evaluation. *Cornea* **35**, 557–561.
9. Kling S, Hafezi F. 2017 An algorithm to predict the biomechanical stiffening effect in corneal crosslinking. *Journal of Refractive Surgery* **33**, 128 – 136. (10.3928/1081597X-20161206-01)
10. Boschetti F, Conti D, Soriano EM, Mazzotta C, Pandolfi A. 2021 Experimental in-vitro investigation on Epi-Off-Crosslinking on porcine corneas. *Plos one* **16**, e0249949.
11. Mazzotta C, Wollensak G, Raiskup F, Pandolfi A, Spoerl E. 2019 The meaning of the demarcation line after riboflavin-UVA corneal collagen crosslinking. *Expert Review of Ophthalmology* **14**, 115–131.
12. Seifert J, Hammer CM, Rheinlaender J, Sel S, Scholz M, Paulsen F, Schäffer TE. 2014 Distribution of Young's modulus in porcine corneas after riboflavin/UVA-induced collagen cross-linking as measured by atomic force microscopy. *PLoS One* **9**, e88186.
13. Cornaggia A, Boschetti F, Mazzotta C, Pandolfi A. 2020 Numerical investigation on epi-off crosslinking effects on porcine corneas. *Mechanics of Soft Materials* **2**, 1–15. (10.1007/s42558-020-00030-7)
14. Kling S, Remon L, Pérez-Escudero A, Merayo-Lloves J, Marcos S. 2010 Corneal biomechanical changes after collagen cross-linking from porcine eye inflation experiments. *Investigative ophthalmology & visual science* **51**, 3961–3968.
15. Timoshenko S, Woinowsky-Krieger S et al.. 1959 *Theory of plates and shells* vol. 2. McGraw-hill New York.
16. Petsche SJ, Pinsky PM. 2013 The role of 3-D collagen organization in stromal elasticity: a model based on X-ray diffraction data and second harmonic-generated images. *Biomechanics and modeling in mechanobiology* **12**, 1101–1113.
17. Pandolfi A, Vasta M. 2012 Fiber distributed hyperelastic modeling of biological tissues. *Mechanics of Materials* **44**, 151–162.
18. Sánchez P, Moutsouris K, Pandolfi A. 2014 Biomechanical and optical behavior of human corneas before and after photorefractive keratectomy. *Journal of Cataract & Refractive Surgery* **40**, 905–917.
19. Montanino A, Gizzi A, Vasta M, Angelillo M, Pandolfi A. 2018 Modeling the biomechanics of the human cornea accounting for local variations of the collagen fibril architecture. *ZAMM-Journal of Applied Mathematics and Mechanics/Zeitschrift für Angewandte Mathematik und Mechanik* **98**, 2122–2134.
20. Pandolfi A, Boschetti F. 2015 The influence of the geometry of the porcine cornea on the biomechanical response of inflation tests. *Computer methods in biomechanics and biomedical engineering* **18**, 64–77.
21. Pandolfi A, Manganiello F. 2006 A model for the human cornea: constitutive formulation and numerical analysis. *Biomechanics and modeling in mechanobiology* **5**, 237–246.

## A. Constitutive model of the stroma

We use a hyperelastic finite kinematics anisotropic constitutive model of the human cornea, described first in parametric form in [21] and extended to a stochastic material in [17]. The model has been adapted to the structure of pig eyes [20] and already employed to model crosslinked pig corneas in [13]. The material model accounts for the presence of the collagen fibrils, described in terms of two distributed families of fibrils following a von Mises distribution [17], in order to characterize the material with a certain degree of uncertainty. The material is a composite, with collagen fibrils embedded in an isotropic matrix of proteoglycans and elastin. The strain energy density splits additively into volumetric, isotropic-iscochoric, and anisotropic-isochoric parts as

$$\Psi = \Psi_{\rm vol}(J) + \Psi_{\rm iso}(\overline{I}_1, \overline{I}_2) + \Psi_{\rm aniso}(\overline{I}^*_{4\,M}, \sigma^2_{I_4\,M})\,,$$

where $\mathbf{F} = d\mathbf{x}/d\mathbf{X}$ is the deformation gradient, $\mathbf{x}$ denotes the current coordinates and $\mathbf{X}$ the reference coordinates, and $J = \det \mathbf{F}$ is the Jacobian determinant. We denote with $\overline{\mathbf{C}} = \overline{\mathbf{F}}^T\overline{\mathbf{F}} = J^{-2/3}\mathbf{F}^T\mathbf{F}$ the isochoric Cauchy-Green deformation tensor, and assume that the two distributions $M = 1, 2$ of collagen fibrils have a main orientation $\mathbf{a}_M$. The arguments of the

volumetric and isotropic strain energy densities are the first and the second modified invariants of $\overline{\mathbf{C}}$

$$\overline{I}_1 = \mathrm{tr}\overline{\mathbf{C}}\,, \qquad \overline{I}_2 = 1/2\left[(\mathrm{tr}\overline{\mathbf{C}})^2 - \mathrm{tr}\overline{\mathbf{C}}^2)\right]\,,$$

where $\mathrm{tr}(.)$ denotes the trace operator. The average pseudo-invariant $\overline{I}^*_{4\,M}$ is defined as

$$\overline{I}^*_{4\,M} = [\kappa_M \mathbf{I} + (1-3\kappa_M)\mathbf{a}_M \otimes \mathbf{a}_M] : \overline{\mathbf{C}}$$

where $\kappa_M$ is a dispersion parameter that derives analytically from the fibril dispersion function, $\otimes$ denotes the tensor product, and $(:)$ denotes the double contraction product. The variance operator $\sigma^2_{I_4\,M}$ is defined as

$$\sigma^2_{I_4\,M} = \overline{\mathbf{C}} : \mathbf{a}_M \otimes \mathbf{a}_M \otimes \mathbf{a}_M \otimes \mathbf{a}_M : \overline{\mathbf{C}} - \overline{I}^*_{4\,M}$$

The explicit expressions of the energies used in the model are

$$\Psi_{\mathrm{vol}} = \frac{1}{4}K\left(J^2 - 1 - 2\log J\right)\,,$$

$$\Psi_{\mathrm{iso}} = \frac{1}{2}\left[\mu_1\left(\overline{I}_1 - 3\right) + \mu_2\left(\overline{I}_2 - 3\right)\right]\,, \quad \mu_1 + \mu_2 = \mu\,,$$

$$\Psi_{\mathrm{aniso}} = \sum_{M=1}^{2} \frac{k_{1\,M}}{2\,k_{2\,M}}\left[\exp D^*\left(\overline{I}^*_{4\,M}\right) - 1\right]\left(1 + K^*\sigma^2_{I_4\,M}\right)\,,$$

where $K$ is the bulk modulus, $\mu = \mu_1 + \mu_2$ is the shear modulus of the soft isotropic matrix, while $k_{1\,M}$ (stiffness-like parameter) and $k_{2\,M}$ (dimensionless rigidity parameters) control the mechanical response of the reinforcing fibers at low and high strains, respectively. The coefficient $D^*(\overline{I}^*_{4\,M})$ reads

$$D^*\left(\overline{I}^*_{4\,M}\right) = k_{2\,M}\left(\overline{I}^*_{4\,M} - 1\right)^2\,,$$

and the coefficient $K^*$

$$k^* = k_{2\,M}\left[1 + 2D^*\left(\overline{I}^*_{4\,M}\right)\right]\,.$$

In summary, the parameters of the model, for every material point, are seven; five with the dimension of a stiffness (elastic moduli), i. e., $K$, $\mu_1$, $\mu_2$, $k_{1\,1}$, $k_{1\,2}$ and two dimensionless rigidity coefficients $k_{2\,1}$, $k_{2\,2}$. More details can be found in the original work [17].

## B. Material data for the layers of cornea

| Pre-operative | | | | | |
|---|---|---|---|---|---|
| Time (min) | Layer | $\mu_1$ (MPa) | $\mu_2$ (MPa) | $k_{11}, k_{12}$ (MPa) | $k_{21}, k_{22}$ |
| 2.5 | 1 | 0.0100 | -0.0090 | 0.120 | 200 |
| | 2 | 0.0118 | -0.0106 | 0.142 | 236 |
| | 3 | 0.0136 | -0.0123 | 0.164 | 273 |
| | 4 | 0.0155 | -0.0139 | 0.186 | 309 |
| | 5 | 0.0173 | -0.0155 | 0.207 | 345 |
| | 6 | 0.0191 | -0.0172 | 0.229 | 382 |
| | 7 | 0.0209 | -0.0188 | 0.251 | 418 |
| | 8 | 0.0227 | -0.0205 | 0.273 | 455 |
| | 9 | 0.0245 | -0.0221 | 0.295 | 491 |
| | 10 | 0.0264 | -0.0237 | 0.316 | 527 |
| 5.0 | 1 | 0.0100 | -0.0090 | 0.160 | 200 |
| | 2 | 0.0118 | -0.0106 | 0.189 | 236 |
| | 3 | 0.0136 | -0.0123 | 0.218 | 273 |
| | 4 | 0.0155 | -0.0139 | 0.247 | 309 |
| | 5 | 0.0173 | -0.0155 | 0.276 | 345 |
| | 6 | 0.0191 | -0.0172 | 0.306 | 382 |
| | 7 | 0.0209 | -0.0188 | 0.335 | 418 |
| | 8 | 0.0227 | -0.0205 | 0.364 | 455 |
| | 9 | 0.0245 | -0.0221 | 0.393 | 491 |
| | 10 | 0.0264 | -0.0237 | 0.422 | 527 |
| 10 | 1 | 0.0100 | -0.0090 | 0.130 | 200 |
| | 2 | 0.0118 | -0.0106 | 0.154 | 236 |
| | 3 | 0.0136 | -0.0123 | 0.177 | 273 |
| | 4 | 0.0155 | -0.0139 | 0.201 | 309 |
| | 5 | 0.0173 | -0.0155 | 0.225 | 345 |
| | 6 | 0.0191 | -0.0172 | 0.248 | 382 |
| | 7 | 0.0209 | -0.0188 | 0.272 | 418 |
| | 8 | 0.0227 | -0.0205 | 0.296 | 455 |
| | 9 | 0.0245 | -0.0221 | 0.319 | 491 |
| | 10 | 0.0264 | -0.0237 | 0.343 | 527 |
| 15 | 1 | 0.0100 | -0.0090 | 0.220 | 200 |
| | 2 | 0.0118 | -0.0106 | 0.260 | 236 |
| | 3 | 0.0136 | -0.0123 | 0.300 | 273 |
| | 4 | 0.0155 | -0.0139 | 0.340 | 309 |
| | 5 | 0.0173 | -0.0155 | 0.380 | 345 |
| | 6 | 0.0191 | -0.0172 | 0.420 | 382 |
| | 7 | 0.0209 | -0.0188 | 0.460 | 418 |
| | 8 | 0.0227 | -0.0205 | 0.500 | 455 |
| | 9 | 0.0245 | -0.0221 | 0.540 | 491 |
| | 10 | 0.0264 | -0.0237 | 0.580 | 527 |
| 20 | 1 | 0.0100 | -0.0090 | 0.140 | 300 |
| | 2 | 0.0118 | -0.0106 | 0.166 | 355 |
| | 3 | 0.0136 | -0.0123 | 0.191 | 409 |
| | 4 | 0.0155 | -0.0139 | 0.216 | 464 |
| | 5 | 0.0173 | -0.0155 | 0.242 | 518 |
| | 6 | 0.0191 | -0.0172 | 0.267 | 573 |
| | 7 | 0.0209 | -0.0188 | 0.293 | 627 |
| | 8 | 0.0227 | -0.0205 | 0.318 | 682 |
| | 9 | 0.0245 | -0.0221 | 0.344 | 736 |
| | 10 | 0.0264 | -0.0237 | 0.369 | 791 |

**Table 3.** Pre-operative material modelling parameters for each layer (from posterior–layer 1–to anterior–layer 10) for the five groups–treatment duration.

| Post-operative - Case 1: Full linear | | | | | |
|---|---|---|---|---|---|
| Time (min) | Layer | $\mu_1$ (MPa) | $\mu_2$ (MPa) | $k_{11}, k_{12}$ (MPa) | $k_{21}, k_{22}$ |
| 2.5 | 1 | 0.0100 | -0.0090 | 0.120 | 200 |
| | 2 | 0.0137 | -0.0123 | 0.165 | 274 |
| | 3 | 0.0174 | -0.0157 | 0.209 | 349 |
| | 4 | 0.0212 | -0.0190 | 0.254 | 423 |
| | 5 | 0.0249 | -0.0224 | 0.299 | 497 |
| | 6 | 0.0286 | -0.0257 | 0.343 | 572 |
| | 7 | 0.0323 | -0.0291 | 0.388 | 646 |
| | 8 | 0.0360 | -0.0324 | 0.432 | 720 |
| | 9 | 0.0397 | -0.0358 | 0.477 | 795 |
| | 10 | 0.0435 | -0.0391 | 0.522 | 869 |
| 5.0 | 1 | 0.0100 | -0.0090 | 0.200 | 200 |
| | 2 | 0.0132 | -0.0119 | 0.264 | 264 |
| | 3 | 0.0164 | -0.0147 | 0.328 | 328 |
| | 4 | 0.0196 | -0.0176 | 0.392 | 391 |
| | 5 | 0.0228 | -0.0205 | 0.455 | 455 |
| | 6 | 0.0260 | -0.0234 | 0.519 | 519 |
| | 7 | 0.0291 | -0.0262 | 0.583 | 583 |
| | 8 | 0.0323 | -0.0291 | 0.647 | 647 |
| | 9 | 0.0355 | -0.0320 | 0.711 | 711 |
| | 10 | 0.0387 | -0.0348 | 0.774 | 774 |
| 10 | 1 | 0.0100 | -0.0090 | 0.130 | 200 |
| | 2 | 0.0145 | -0.0130 | 0.188 | 289 |
| | 3 | 0.0189 | -0.0170 | 0.246 | 379 |
| | 4 | 0.0234 | -0.0211 | 0.304 | 468 |
| | 5 | 0.0279 | -0.0251 | 0.362 | 557 |
| | 6 | 0.0323 | -0.0291 | 0.420 | 646 |
| | 7 | 0.0368 | -0.0331 | 0.478 | 736 |
| | 8 | 0.0412 | -0.0371 | 0.536 | 825 |
| | 9 | 0.0457 | -0.0411 | 0.594 | 914 |
| | 10 | 0.0502 | -0.0452 | 0.652 | 1004 |
| 15 | 1 | 0.0100 | -0.0090 | 0.220 | 200 |
| | 2 | 0.0146 | -0.0131 | 0.320 | 291 |
| | 3 | 0.0191 | -0.0172 | 0.421 | 382 |
| | 4 | 0.0237 | -0.0213 | 0.521 | 474 |
| | 5 | 0.0282 | -0.0254 | 0.622 | 565 |
| | 6 | 0.0328 | -0.0295 | 0.722 | 656 |
| | 7 | 0.0374 | -0.0336 | 0.822 | 747 |
| | 8 | 0.0419 | -0.0377 | 0.923 | 839 |
| | 9 | 0.0465 | -0.0418 | 1.023 | 930 |
| | 10 | 0.0511 | -0.0460 | 1.123 | 1021 |
| 20 | 1 | 0.0100 | -0.0090 | 0.140 | 300 |
| | 2 | 0.0168 | -0.0151 | 0.235 | 504 |
| | 3 | 0.0236 | -0.0213 | 0.331 | 709 |
| | 4 | 0.0304 | -0.0274 | 0.426 | 913 |
| | 5 | 0.0372 | -0.0335 | 0.521 | 1117 |
| | 6 | 0.0441 | -0.0396 | 0.617 | 1322 |
| | 7 | 0.0509 | -0.0458 | 0.712 | 1526 |
| | 8 | 0.0577 | -0.0519 | 0.807 | 1730 |
| | 9 | 0.0645 | -0.0580 | 0.903 | 1935 |
| | 10 | 0.0713 | -0.0642 | 0.998 | 2139 |

**Table 4.** Post-operative material modelling parameters for each layer (from posterior–layer 1–to anterior–layer 10) for the different treatment duration when a fully linear distribution is assumed for the treatment effect.

| Post-operative - Case 2: 1/3 linear | | | | | |
|---|---|---|---|---|---|
| Time (min) | Layer | $\mu_1$ (MPa) | $\mu_2$ (MPa) | $k_{11}, k_{12}$ (MPa) | $k_{21}, k_{22}$ |
| 2.5 | 1 | 0.0100 | -0.0090 | 0.120 | 200 |
| | 2 | 0.0118 | -0.0106 | 0.142 | 236 |
| | 3 | 0.0136 | -0.0123 | 0.164 | 273 |
| | 4 | 0.0155 | -0.0139 | 0.186 | 309 |
| | 5 | 0.0173 | -0.0155 | 0.207 | 345 |
| | 6 | 0.0191 | -0.0172 | 0.229 | 382 |
| | 7 | 0.0209 | -0.0188 | 0.251 | 418 |
| | 8 | 0.0402 | -0.0362 | 0.483 | 805 |
| | 9 | 0.0630 | -0.0567 | 0.757 | 1261 |
| | 10 | 0.0859 | -0.0773 | 1.030 | 1717 |
| 5.0 | 1 | 0.0100 | -0.0090 | 0.200 | 200 |
| | 2 | 0.0118 | -0.0106 | 0.236 | 236 |
| | 3 | 0.0136 | -0.0123 | 0.273 | 273 |
| | 4 | 0.0155 | -0.0139 | 0.309 | 309 |
| | 5 | 0.0173 | -0.0155 | 0.346 | 345 |
| | 6 | 0.0191 | -0.0172 | 0.382 | 382 |
| | 7 | 0.0209 | -0.0188 | 0.418 | 418 |
| | 8 | 0.0350 | -0.0315 | 0.700 | 700 |
| | 9 | 0.0515 | -0.0463 | 1.030 | 1030 |
| | 10 | 0.0680 | -0.0612 | 1.360 | 1360 |
| 10 | 1 | 0.0100 | -0.0090 | 0.130 | 200 |
| | 2 | 0.0118 | -0.0106 | 0.154 | 236 |
| | 3 | 0.0136 | -0.0123 | 0.177 | 273 |
| | 4 | 0.0155 | -0.0139 | 0.201 | 309 |
| | 5 | 0.0173 | -0.0155 | 0.225 | 345 |
| | 6 | 0.0191 | -0.0172 | 0.248 | 382 |
| | 7 | 0.0209 | -0.0188 | 0.272 | 418 |
| | 8 | 0.0483 | -0.0434 | 0.628 | 965 |
| | 9 | 0.0807 | -0.0727 | 1.050 | 1615 |
| | 10 | 0.1132 | -0.1019 | 1.472 | 2264 |
| 15 | 1 | 0.0100 | -0.0090 | 0.220 | 200 |
| | 2 | 0.0118 | -0.0106 | 0.260 | 236 |
| | 3 | 0.0136 | -0.0123 | 0.300 | 273 |
| | 4 | 0.0155 | -0.0139 | 0.340 | 309 |
| | 5 | 0.0173 | -0.0155 | 0.380 | 345 |
| | 6 | 0.0191 | -0.0172 | 0.420 | 382 |
| | 7 | 0.0209 | -0.0188 | 0.460 | 418 |
| | 8 | 0.0494 | -0.0445 | 1.087 | 988 |
| | 9 | 0.0832 | -0.0749 | 1.831 | 1664 |
| | 10 | 0.1170 | -0.1053 | 2.574 | 2340 |
| 20 | 1 | 0.0100 | -0.0090 | 0.140 | 300 |
| | 2 | 0.0118 | -0.0106 | 0.166 | 355 |
| | 3 | 0.0136 | -0.0123 | 0.191 | 409 |
| | 4 | 0.0155 | -0.0139 | 0.216 | 464 |
| | 5 | 0.0173 | -0.0155 | 0.242 | 518 |
| | 6 | 0.0191 | -0.0172 | 0.267 | 573 |
| | 7 | 0.0209 | -0.0188 | 0.293 | 627 |
| | 8 | 0.0795 | -0.0716 | 1.113 | 2385 |
| | 9 | 0.1495 | -0.1345 | 2.092 | 4484 |
| | 10 | 0.2194 | -0.1975 | 3.072 | 6582 |

**Table 5.** Post-operative material modelling parameters for each layer (from posterior–layer 1–to anterior–layer 10) for the different treatment duration when a 1/3 linear distribution is assumed for the treatment effect.

| Post-operative - Case 3: time-dependent | | | | | |
|---|---|---|---|---|---|
| Time (min) | Layer | $\mu_1$ (MPa) | $\mu_2$ (MPa) | $k_{11}, k_{12}$ (MPa) | $k_{21}, k_{22}$ |
| 2.5 | 1 | 0.0100 | -0.0090 | 0.120 | 200 |
| | 2 | 0.0118 | -0.0106 | 0.142 | 236 |
| | 3 | 0.0136 | -0.0123 | 0.164 | 273 |
| | 4 | 0.0155 | -0.0139 | 0.186 | 309 |
| | 5 | 0.0173 | -0.0155 | 0.207 | 345 |
| | 6 | 0.0191 | -0.0172 | 0.229 | 382 |
| | 7 | 0.0209 | -0.0188 | 0.251 | 418 |
| | 8 | 0.0402 | -0.0362 | 0.483 | 805 |
| | 9 | 0.0630 | -0.0567 | 0.757 | 1261 |
| | 10 | 0.0859 | -0.0773 | 1.030 | 1717 |
| 5.0 | 1 | 0.0100 | -0.0090 | 0.200 | 200 |
| | 2 | 0.0118 | -0.0106 | 0.236 | 236 |
| | 3 | 0.0136 | -0.0123 | 0.273 | 273 |
| | 4 | 0.0155 | -0.0139 | 0.309 | 309 |
| | 5 | 0.0173 | -0.0155 | 0.346 | 345 |
| | 6 | 0.0191 | -0.0172 | 0.382 | 382 |
| | 7 | 0.0209 | -0.0188 | 0.418 | 418 |
| | 8 | 0.0350 | -0.0315 | 0.700 | 700 |
| | 9 | 0.0515 | -0.0463 | 1.030 | 1030 |
| | 10 | 0.0680 | -0.0612 | 1.360 | 1360 |
| 10 | 1 | 0.0100 | -0.0090 | 0.130 | 200 |
| | 2 | 0.0117 | -0.0105 | 0.152 | 233 |
| | 3 | 0.0133 | -0.0120 | 0.173 | 267 |
| | 4 | 0.0150 | -0.0135 | 0.195 | 300 |
| | 5 | 0.0167 | -0.0150 | 0.217 | 333 |
| | 6 | 0.0183 | -0.0165 | 0.238 | 366 |
| | 7 | 0.0259 | -0.0233 | 0.337 | 518 |
| | 8 | 0.0473 | -0.0426 | 0.615 | 946 |
| | 9 | 0.0794 | -0.0714 | 1.032 | 1587 |
| | 10 | 0.1130 | -0.1017 | 1.469 | 2260 |
| 15 | 1 | 0.0100 | -0.0090 | 0.220 | 200 |
| | 2 | 0.0117 | -0.0105 | 0.257 | 233 |
| | 3 | 0.0133 | -0.0120 | 0.293 | 267 |
| | 4 | 0.0150 | -0.0135 | 0.330 | 300 |
| | 5 | 0.0167 | -0.0150 | 0.366 | 333 |
| | 6 | 0.0183 | -0.0165 | 0.403 | 366 |
| | 7 | 0.0242 | -0.0217 | 0.531 | 483 |
| | 8 | 0.0397 | -0.0358 | 0.874 | 795 |
| | 9 | 0.0754 | -0.0678 | 1.658 | 1507 |
| | 10 | 0.1994 | -0.1795 | 4.388 | 3989 |
| 20 | 1 | 0.0100 | -0.0090 | 0.140 | 300 |
| | 2 | 0.0117 | -0.0105 | 0.163 | 350 |
| | 3 | 0.0133 | -0.0120 | 0.187 | 400 |
| | 4 | 0.0150 | -0.0135 | 0.210 | 450 |
| | 5 | 0.0167 | -0.0150 | 0.233 | 500 |
| | 6 | 0.0183 | -0.0165 | 0.257 | 550 |
| | 7 | 0.0253 | -0.0228 | 0.354 | 759 |
| | 8 | 0.0447 | -0.0402 | 0.626 | 1341 |
| | 9 | 0.0896 | -0.0807 | 1.255 | 2688 |
| | 10 | 0.7160 | -0.6444 | 10.024 | 21480 |

**Table 6.** Post-operative material modelling parameters for each layer (from posterior–layer 1–to anterior–layer 10) for the different treatment duration when a time-dependent distribution is assumed for the treatment effect.